Input Design and Recommendations for the Identification of Hysteretic NARX Models ⋆

Lucas A. Tavares * **Petrus E. O. G. B. Abreu** * **Luis A. Aguirre** *

* *Graduate Program in Electrical Engineering, Universidade Federal de Minas Gerais, Belo Horizonte, MG, Brazil (e-mails: amarallucas@ufmg.br, petrusabreu@ufmg.br, aguirre@ufmg.br)*

Abstract: This paper deals with key-aspects in the identification of Nonlinear AutoRegressive models with eXogenous inputs (NARX), with a particular attention to system with hysteresis. The main contribution is the mathematical description of a class of input signals with dominant spectral power in a specified frequency range and that are able to drive the system to different operating points. Other important contribution is the discussion about the influence of some identification meta-parameters and structural constraints under the predictive performance of NARX models in the context of hysteretic systems. The identification procedure is illustrated with two numerical and one experimental examples, a pneumatic valve with hysteresis-type nonlinearity. NARX models are built which, due to their simplicity, are promising for applications in nonlinearity compensation problems.

Keywords: Design Excitation Inputs; System Identification; NARX models; Hysteresis.

1. INTRODUCTION

For many control applications, the first step is the identification of a valid model. The identification process can be addressed from *black-box* or *gray-box* perspectives. In the black-box approach, the system is modeled exclusively from measured data whereas gray-box techniques also use auxiliary information about the system (Aguirre, 2019).

In this sense, it is necessary to define the mathematical representation of the models, such as differential equations (Lin et al., 2013), neural networks (NNs) (Meng et al., 2020), nonlinear autoregressive models with exogenous inputs (NARX) (Billings, 2013), among others. Once the mathematical representation is selected, the next step is to collect and prepare the data set for identification purposes. Thus, it is essential to define an input that will properly excite the system for collecting representative data.

The next task is to select the model structure (Billings, 2013), which consists of choosing from a large set of candidates which will be part of the model. In the sequel, parameters are estimated with some optimization algorithm. The last step is model validation, which requires different data from those used in the previous steps.

A critical part of the identification process is the design of an appropriate excitation input (Billings, 2013). In related works (Martins and Aguirre, 2016; Abreu et al., 2020) inputs were produced with filtered Gaussian noise. It has been found that such inputs not always produce best results. In order to overcome this shortcoming, a specific procedure has been devised in which the user can specify not only particular frequency ranges but also specific operating points. One of the aims of this paper is to describe such a procedure. In the sequel two well established techniques are used for structure selection. The Error Reduction Ratio (ERR) (Korenberg et al., 1987) aims to sort the most representative regressors in the model, while Akaike's Information Criterion (AIC) (Akaike, 1974) is used to determine the number of terms. The Extended Least Squares (ELS) algorithm (Ljung, 1999) is used to estimate the parameters for the chosen structure.

Three systems are used for illustration purposes. The first one is a simulated heat system with a polynomial nonlinearity. For this example, we discuss the impact of the increased noise on the model predictive accuracy. A discussion about the benefits of gray-box approaches is presented in the second example, which is a Bouc-Wen model that describes the hysteretic behavior in a piezoelectric actuator. We compare results from black-box approaches, with those proposed in (Martins and Aguirre, 2016) and (Abreu et al., 2020). Finally, the last example is an experimental pneumatic valve where we compare models obtained in the literature with those identified in this paper. An interesting issue is how the constraints used in (Abreu et al., 2020) affect the NARX models predictive accuracy. The improvements obtained here are related to an appropriate choice of the meta-parameters and the use of non-biased estimators.

The main contributions of this work are: i) to describe a procedure to design suitable inputs that can reach various operating points and can preserve the frequencies of interest, and ii) to put forward practical recommendations about the identification of NARX models for hysteretic systems. It is worth mentioning that the models identified here have simple and representative structures, which is an appealing feature for compensator design purposes.

⋆ PEOGBA and LAA gratefully acknowledge financial support from CNPq (Grant Nos. 142194/2017-4 and 303412/2019-4) and FAPEMIG (TEC-1217/98).

This paper is organized as follows. Section 2 presents the fundamental theoretical aspects, while Sec. 3 summarizes the identification methodology. The numerical and experimental examples are in Sec. 4. Section 5 provides the concluding remarks.

2. BACKGROUND

Consider a data set $Z^N=\{u(k), y_s(k)\}_{k=1}^N$, with $N\in\mathbb{N}^+$ samples, obtained by measuring the continuous input $u(t)\in\mathbb{R}$ and output $y_s(t)\in\mathbb{R}$ signals from a nonlinear dynamical system $\mathcal{S}$, at sampling time T_s. The aim is to identify a Nonlinear AutoRegressive model with eXogenous inputs (NARX), namely $\mathcal{M}$, to represent the relevant nonlinear aspects of $\mathcal{S}$ (Leontaritis and Billings, 1985):

$$y(k)=f^\ell\big(y(k-1),\ldots,y(k-n_y),u(k-\tau_\mathrm{d}),\ldots,u(k-n_u)\big), \quad (1)$$

where $y(k)\in\mathbb{R}$ is the model output that predicts $y_s(k)$, and $f^\ell(\cdot)$ is a nonlinear polynomial function with degree $\ell\in\mathbb{N}^+$. $n_u, n_y\in\mathbb{N}^+$ are the maximum lags for u and y, respectively, and $\tau_\mathrm{d}\in\mathbb{N}^+$ is the pure time delay.

Considering the modeling error of $\mathcal{M}$ or residues, i.e. $\xi(k)=y_s(k)-y(k)$, the following equation can be found:

$$y_s(k) = \boldsymbol{\psi}^T(k-1)\hat{\boldsymbol{\theta}} + \xi(k), \quad (2)$$

where $\hat{\boldsymbol{\theta}}\in\mathbb{R}^{n_\theta}$ is the parameter vector, $\boldsymbol{\psi}(k-1)\in\mathbb{R}^{n_\theta}$ is the regressor vector, whose j-th term $\psi_j(k-1)\in\mathbb{R}$ corresponds to linear or nonlinear combinations up to degree ℓ of the variables $y(k-k_y)$, $k_y\in\{1,\ldots,n_y\}$, and $u(k-k_u)$, $k_u\in\{\tau_d,\ldots,n_u\}$, while T indicates the transpose. Applying (2), for $k=1,\ldots,N$, over the data set Z^N, it is possible to build the following equation in matrix form (Aguirre, 2019):

$$\boldsymbol{y} = \boldsymbol{\Psi}\hat{\boldsymbol{\theta}} + \boldsymbol{\xi}, \quad (3)$$

where $\boldsymbol{\xi}\triangleq[\xi(1),\ldots,\xi(N)]^T\in\mathbb{R}^N$ is the residual vector, $\boldsymbol{y}\triangleq[y_s(1),\ldots,y_s(N)]^T\in\mathbb{R}^N$ is the vector of output measurements, and $\boldsymbol{\Psi}\triangleq[\boldsymbol{\psi}_1,\ldots,\boldsymbol{\psi}_{n_\theta}]\in\mathbb{R}^{N\times n_\theta}$ is the regressor matrix composed by the regressors vectors $\boldsymbol{\psi}_j\triangleq[\psi_j(1),\ldots,\psi_j(N)]^T\in\mathbb{R}^N$, whose j-th term is defined as detailed above for (2). As (3) is linear in the parameters, classic regression methods can be used, e.g. Least Squares (LS). The LS method provides the following parameter vector $\hat{\boldsymbol{\theta}}_\mathrm{LS}$ optimal, in the sense of least squares of the modeling error:

$$\hat{\boldsymbol{\theta}}_\mathrm{LS} = [\boldsymbol{\Psi}^T\boldsymbol{\Psi}]^{-1}\boldsymbol{\Psi}^T\boldsymbol{y}. \quad (4)$$

When $\xi(k)$ is autocorrelated, the LS method is biased. It tends to occur with the effects of noise, being the addition of *moving average* (MA) terms a way to circumvent this issue. However, this addition provides a nonlinear model in the parameters, and the classic LS cannot be used. Fortunately, there is a well established alternative to deal with this problem that is the Extended Least Squares (ELS) method (Billings, 2013). This iterative algorithm uses $\xi(k)$ from the previous iteration to extend the regressor matrix, being executed until a convergence criterion is reached, as illustrated by the following steps (Ljung, 1999):

1. Based on Eq. (4), estimate $\hat{\boldsymbol{\theta}}_\mathrm{LS}$;
2. Calculate the vector of residues, $\boldsymbol{\xi}_1=\boldsymbol{y}-\boldsymbol{\Psi}\hat{\boldsymbol{\theta}}_\mathrm{LS}$;
3. Define the iteration $i=2$ and the convergence limit $\zeta\in\mathbb{R}^+$;
4. Build $\tilde{\boldsymbol{\Psi}}_i=[\boldsymbol{\Psi}\,\vdots\,\boldsymbol{\xi}_{i-1}]$, the extended regression matrix;
5. Estimate via LS the new vector of parameters at each iteration: $\hat{\boldsymbol{\theta}}_{\mathrm{ELS}_i}=[\tilde{\boldsymbol{\Psi}}_i^T\tilde{\boldsymbol{\Psi}}_i]^{-1}\tilde{\boldsymbol{\Psi}}_i^T\boldsymbol{y}$;
6. Determine the current residues: $\boldsymbol{\xi}_i=\boldsymbol{y}-\tilde{\boldsymbol{\Psi}}_{\boldsymbol{i}}\hat{\boldsymbol{\theta}}_{\mathrm{ELS}_i}$;
7. If $||\hat{\boldsymbol{\theta}}_{\mathrm{ELS}_i}-\hat{\boldsymbol{\theta}}_{\mathrm{ELS}_{i-1}}||_2<\zeta$, make $\hat{\boldsymbol{\theta}}_\mathrm{ELS}=\hat{\boldsymbol{\theta}}_{\mathrm{ELS}_i}$ and finish the process. Otherwise, make $i=i+1$ and return to step 4. $||\bullet||_2$ is the quadratic norm.

The technique described above for determining the parameters must be applied to a previously identified structure. The selection of this structure for $\mathcal{M}$ can be done by combining both techniques described below.

2.1 The Error Reduction Ratio Method

The Error Reduction Ratio (ERR) quantifies the contribution of each term in explaining the data variance (Korenberg et al., 1987). To compute the ERR, each model regressor must be orthogonal to the data, which can be achieved with the Householder transformation (Householder, 1958). Taking the average value of $y_s(k)^2$ on the data, it is possible to find the following expression (Billings, 2013):

$$\frac{1}{N}\sum_{k=1}^{N} y_s(k)^2 = \frac{1}{N}\sum_{i=1}^{n_\theta}\hat{\theta}_i^2\boldsymbol{w_i}^{\boldsymbol{T}}\boldsymbol{w_i} + \frac{1}{N}\boldsymbol{\xi}^{\boldsymbol{T}}\boldsymbol{\xi}, \quad (5)$$

where $\boldsymbol{w_i}=[w_i(1)\ldots w_i(N)]$ is the vector of regressors w_i that are orthogonal to the identification data set. Thus, the ERR due to the inclusion of the i-th regressor is:

$$[\mathrm{ERR}]_i = \frac{\hat{\theta}_i^2\boldsymbol{w_i}^{\boldsymbol{T}}\boldsymbol{w_i}}{\boldsymbol{y}^{\boldsymbol{T}}\boldsymbol{y}}. \quad (6)$$

The inclusion of each term in the model reduces the variance of the modeling error. The index $[\mathrm{ERR}]_i$ quantifies the contribution of the i-th term in the reduction of this variance. By selecting the regressors that provide the highest values for this index, it is possible to reduce the candidate set. This is relevant because the number of candidate regressors tends to increase considerably with the rise of ℓ (Billings, 2013). However, this technique only sorts the candidate terms hierarchically, it is still necessary to choose the number of candidate terms.

2.2 The Akaike's Information Criterion

The Akaike's Information Criterion (AIC) helps to define the number of terms to be included in the model, by minimizing a cost function (Akaike, 1974). The addition of new terms increases the model complexity, which allows a better fit. Considering that the terms were sorted with ERR, a given number of terms n_θ is enough to determine $\mathcal{M}_{n_\theta}$ with an output $y_{n_\theta}(k)$. The variance of the residues, $\sigma_\xi^2(n_\theta)$, tends to reduce when n_θ increases, but this is no guarantee of a better generalization performance. Thus, the AIC is:

$$J_\mathrm{AIC}(n_\theta) = N\ln[\sigma_\xi^2(n_\theta)] + 2n_\theta, \quad (7)$$

which tends to achieve a minimum for some value of n_θ.

2.3 NARX Hysteresis Modeling

Martins and Aguirre (2016) have shown that the inclusion of any multi-function of the first difference of the input is a sufficient condition for NARX models to predict hysteresis behavior under the excitation of loading-unloading inputs. Typically, it is suitable to include the first difference of the input $\phi_1(k)$=$u(k)-u(k-1)$ and its corresponding sign function, $\phi_2(k)$=sign($\phi_1(k)$) that is a multi-function. A general extended NARX model set $\mathcal{M}_{\rm h}$ is given by (Billings and Chen, 1989):

$$y(k) = g^{\ell}\big(y(k-1), \cdots, y(k-n_y),\, u(k-\tau_{\rm d}), \cdots, u(k-n_u), \phi_1(k-1),\, \phi_2(k-1)\big), \tag{8}$$

where $g^{\ell}(\cdot)$ is a polynomial function of the regressor variables up to degree ℓ, and the other parameters were previously mentioned. Model $\mathcal{M}_{\rm h}$ (8) presents two sets of equilibria under loading-unloading excitations: one for loading with $\phi_2(k)$=1, and one for unloading with $\phi_2(k)$=-1 (Martins and Aguirre, 2016; Abreu et al., 2020).

It has been shown that for $\mathcal{M}_{\rm h}$, some regressors can be excluded, regardless of the lags τ_u and τ_y (Abreu et al., 2020), as summarized below:

(i) $y^p(k-\tau_y)$,$y^p(k-\tau_y)\phi_1(k-\tau_u)^q$, and $y^p(k-\tau_y)\phi_2(k-\tau_u)^q$ for p>1, $\forall q$, (Aguirre and Mendes, 1996),
(ii) $\phi_2^q(k-\tau_u)$ for $q>1$ (Martins and Aguirre, 2016), and
(iii) $y^p(k-\tau_y)u^m(k-\tau_u)$ and $u^m(k-\tau_u)$ $\forall p, m$ (Abreu et al., 2020).

Such constraints are specified for the identification of $\mathcal{M}_{\rm h}$, considering Σ_y, the sum of parameters of all linear output regressors, which is forced to be equal to 1. This set of constraints ensure that the model output remains locked when the reference becomes constant (Abreu et al., 2020).

3. INPUT DESIGN

The procedure proposed here takes into account the need to excite the system in a wide frequency range and reach a variety of operating points (Schoukens and Ljung, 2019). Therefore, the procedure starts with determining the frequencies, $f_i \in \mathbb{R}^+$ for i=$1,\ldots,n$, that will be preserved in the signal. For instance, in the case of hysteretic systems, it is necessary to preserve low-frequency information in the identification data (Ikhouane and Rodellar, 2007). To achieve this type of demand, fifth-order low-pass Butterworth filters, $\mathcal{H}_i(q)$, are designed with a cutoff frequency. In this work, we consider that these filters are applied to a purely random signal $e_i(k)$=$\mathcal{N}(0,1)$, $k=1,2,\ldots N_i$, where $\mathcal{N}(0,1)$ is a standard normal distribution. Organizing the data in a vector, $\boldsymbol{e_i} = [e_i(1) \quad e_i(2) \quad \ldots \quad e_i(N_i)]$, each random signal is conditioned to have 1 as maximum and -1 as minimum as follows:

$$e_i(k) = 2\left(\frac{e_i(k) - \min[\boldsymbol{e}_i]}{\max[\boldsymbol{e}_i] - \min[\boldsymbol{e}_i]}\right) - 1, \tag{9}$$

and its number of samples N_i is specified to have an input signal $u(k)$ with N samples, such that N=N_1+N_2+$\cdots$+N_n.

To ensure that the signal $u(k)$ can achieve a variety of operating regions, operating points $o_j \in \mathbb{R}$ for j=$1,\ldots,v$ are defined. For each o_j, an amplitude G_j is defined around the point. In addition, the values assigned for each number of samples N_i must be defined as multiples of the number of operating points, v. This is necessary since it is intended that each frequency has information around all operating points. In this way, the signal $s_i(k)$ that is a part of $u(k)$ is produced as follows:

$$s_i(k)=\begin{cases} \alpha_{i,1}\mathcal{H}_i(q)e_i(k)+o_1, & k=1,\,2,\,\ldots,\,\dfrac{N_i}{v} \\ \vdots & \vdots \\ \alpha_{i,v}\mathcal{H}_i(q)e_i(k)+o_v, & k=(v-1)\dfrac{N_i}{v}+1, \\ & \quad (v-1)\dfrac{N_i}{v}+2,\,\ldots,N_i. \end{cases} \tag{10}$$

The constants $\alpha_{i,j}$ are set to limit the excursion of the input around each operating point. For a given operating point o_j, we have $\alpha_{i,j}$=$G_j/\max[\boldsymbol{e_i}(k_{i,j})]$ for which $k_{i,j}$ = $(j-1)(N_i/v)+1$,$(j-1)(N_i/v)+2,\ldots,j(N_i/v)$. Applying (10) for i = 1,2,…,n, we get $\boldsymbol{s}_1, \boldsymbol{s}_2, \ldots, \boldsymbol{s}_n$ and $\boldsymbol{u}$ is the horizontal concatenation of these inputs:

$$\boldsymbol{u} = [\boldsymbol{s}_1 \quad \boldsymbol{s}_2 \quad \ldots \quad \boldsymbol{s}_n]^T. \tag{11}$$

Finally, selecting the maximum frequency f_i, the low-pass filter related to this frequency is used to eliminate possible higher frequencies originating from concatenation.

This procedure is performed twice, in order to have different realizations for identification and validation inputs, which are applied to the system for data collection. To achieve more robust experiments, Gaussian noise was added directly to the output to obtain $\sigma_n/\sigma_s = 5\%$, where σ_n is the *standard deviation of the noise*, and σ_s is the *standard deviation of the signal*.

Identification data is produced using the input designed in this section. The ERR and AIC (Sec. 2) are used to determine the model structure and parameters are estimated using the ELS method.

4. EXAMPLES

The identification procedure proposed in Sec. 3 is applied in this section for three examples. The first one refers to a heating system modeled by a Hammerstein model with a polynomial nonlinearity; see Sec.4.1. The second is a Bouc-Wen model that simulates the hysteresis of a piezoelectric (PZT) device (Sec. 4.2). The last one refers to an experimental pneumatic valve; see Sec. 4.3. To assess the prediction performance of the obtained models, we use the Mean Absolute Percentage Error (MAPE) index:

$$\text{MAPE} = \frac{\sum_{k=1}^{N} |y_s(k) - y(k)|}{N|\max(\boldsymbol{y}) - \min(\boldsymbol{y})|}. \tag{12}$$

4.1 A Heating System

Consider a small electrical heater modeled by the following Hammerstein structure (Aguirre et al., 2005):

$$\begin{aligned} y(k) =& \beta_1 y(k-1) + \beta_2 v(k-1) + \beta_3 y(k-2) + \beta_4 v(k-2), \\ v(k) =& p_1 u(k)^2 + p_2 u(k), \end{aligned} \tag{13}$$

where $u(k)$, $0 \le u(k) \le 1$, is the voltage applied to the heater that changes the normalized temperature $y(k)$ that is

affected by a quadratic nonlinearity with output $v(k)$, which is the fictitious intermediate signal that appears in block-oriented models. Since one only has access to the physical signals $u(k)$ and $y(k)$, the identification of block-oriented models is challenging (Aguirre et al., 2005). The data set of such a system is the same considered in (Aguirre et al., 2002), which is available in `https://bit.ly/3iQ6rCF`. Here, we reestimate the parameters of model (13), obtaining: $p_1 = 4.639331 \times 10^{-1}$, $p_2 = 5.435865 \times 10^{-2}$, $\beta_1 = 1.205445$, $\beta_2 = 8.985133 \times 10^{-2}$, $\beta_3 = -3.0877507 \times 10^{-1}$ and $\beta_4 = 9.462358 \times 10^{-3}$. This reestimation was necessary due to the parameters provided in (Aguirre et al., 2005) having few decimal digits, which severely impacts in the results for discrete systems.

The independent term in the second-order polynomial that gives $v(k)$ was omitted to ensure $y = 0$ when $u = 0$. p_1 and p_2 were estimated directly from static data using LS, although β's were estimated from dynamical data using ELS algorithm. The operation region of the model is $u(k) \in [0, 1]$ and $y(k) \in [0, 0.5]$. For (13), the free-run validation result of MAPE is about 1.16%.

Henceforth, the Hammerstein model (13) will be treated as the system $\mathcal{S}$ to be identified using a NARX polynomial model $\mathcal{M}$ (1). The input $u(k)$ was designed as (10) and (11) with: n=2, f_1=0.001Hz, f_2=0.005Hz, v=3, o_1=0.3V, o_2=0.5V, o_3=0.7V, G_1=G_2=G_3=0.2V, N = 2000, N_1=1000, and N_2=1000. Figure 1 shows the Monte Carlo Test results to assess how the predictive capacity of the identified models degrades, using the MAPE index, as the noise power is increased, i.e. σ_n/σ_s (see Sec. 3).

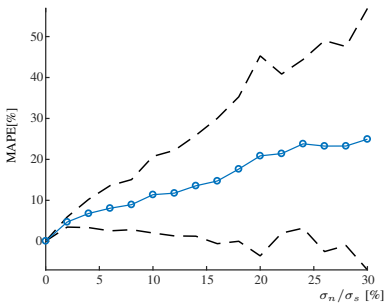

Figure 1. Monte Carlo evaluation, MAPE [%], of models estimated from the identification data under different noise power, σ_n/σ_s [%]. (⊖) is the average of 50 runs, and (- -) refers to ±2 standard deviations.

The Monte Carlo Tests can be summarized as follows. For each test, the system output $y_s(k)$ is added with a Gaussian noise that has a given value of the ratio σ_n/σ_s.The values of σ_n/σ_s vary from 0% to 30% with successive increases of 2%. For each σ_n/σ_s value, 50 perturbed output signals are generated and their respective models are identified considering the previous recommendations. Finally, we compute the mean and standard deviation of MAPE for each σ_n/σ_s value. From Fig. 1, it is possible to see that the model accuracy tends to be damaged as the values of σ_n/σ_s are increased. Also, the predictability is harmed, since there is an enlargement in the confidence intervals.

As mentioned in Sec. 3, a Gaussian noise was added directly to the output to yield a σ_n/σ_s=5%. Taking ℓ=3 and n_y=n_u=3, using the ERR together with the AIC criterion and the ELS for parameter estimation, the following structure is selected for $\mathcal{M}$:

$$y(k) = \hat{\theta}_1 y(k-1) + \hat{\theta}_2 u(k-2)^2 + \hat{\theta}_3 y(k-2), \qquad (14)$$

where $\hat{\theta}_1$=8.958185 × 10^{-1}, $\hat{\theta}_2$=6.393347 × 10^{-2}, and $\hat{\theta}_3$ = −1.746750 × 10^{-2}. The noise-free results for the validation data set are shown in Fig. 2 with a MAPE of about 1.80%.

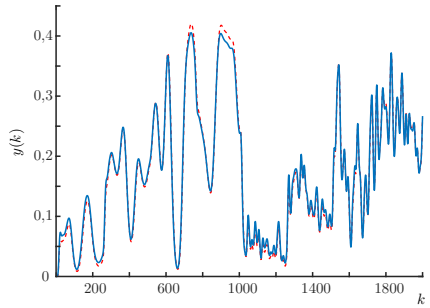

Figure 2. Noise-free validation results for heating system. (–) is the system output $y(k)$ (13), and (- -) is the free-run simulation of model (14).

4.2 A Hysteretic System

Here, the benchmark system is a piezoelectric actuator (PZT), which is an unimorph cantilever, simulated by the Bouc-Wen model given below (Rakotondrabe, 2011):

$$\begin{aligned} \dot{h}(t) =& \alpha_{\text{bw}}\dot{u}(t) - \beta_{\text{bw}}|\dot{u}(t)|h(t) - \gamma_{\text{bw}}\dot{u}(t)|h(t)|, \\ y(t) =& \nu_y u(t) - h(t), \end{aligned} \qquad (15)$$

where $u(t)$[V] is the voltage input, $y(t)[\mu$m] is the position output. The hysteretic loop is determined by α_{bw} = 0.9[μm/V] and β_{bw} = γ_{bw} = 0.008[V^{-1}], while ν_y = 1.6[μm/V] is a weight factor for the output. Then, (15) is now the system $\mathcal{S}$ to be identified and its simulation is done using a fourth-order Runge-Kutta method with integration step δ_t = 5ms.

To compare the different hysteresis modeling strategies, three NARX models are obtained. The excitation input $u(k)$ is designed according to (10) and (11) with: n=2, f_1=0.2Hz, f_2=5Hz, v=2, o_1=o_2=0V, G_1=25V, G_2=50V, N=19200, N_1=16000 and N_2=3200. Gaussian noise was added directly to the output to yield a σ_n/σ_s=5%, as in the previous example. Also, we assume that ℓ=3 and n_y=n_u=1, for the three models, and their structure are chosen using the ERR together with AIC, while the parameters are estimated using the ELS method.

The first model is identified using the *gray-box* recommendations proposed in (Martins and Aguirre, 2016). So, $u(k)$, $y(k)$, $\phi_1(k)$=$u(k)$−$u(k-1)$, and $\phi_2(k)$ = sign($\phi_1(k)$) are chosen as candidate regressors, thus yielding:

$$\begin{aligned} y(k)=&\hat{\theta}_1 y(k-1)+\hat{\theta}_2\phi_1(k-1)\phi_2(k-1)u(k-1) \\ &+\hat{\theta}_3\phi_1(k-1)\phi_2(k-1)y(k-1)+\hat{\theta}_4\phi_1(k-1), \end{aligned} \qquad (16)$$

where $\hat{\theta}_1$=1.000099, $\hat{\theta}_2$=6.630567 × 10^{-3}, $\hat{\theta}_3$=−6.247018 × 10^{-3}, and $\hat{\theta}_4$ = 7.892915. These parameter values combined with structure (16) are referred to here as $\mathcal{M}_{\text{h},1}$.

Based on the recommendations extracted from (Abreu et al., 2020), the second model has the same structure as

model $\mathcal{M}_{\mathrm{h},1}$ (16), since it meets the structural constraints (i), (ii), and (iii) of Sec. 2.3. Conversely, for model (16) to comply with the constraints on the parameters, i.e. to ensure Σ_y=1, we reestimate their parameters with the Constrained Least Squares (CLS) method (Draper and Smith, 1998). Here, it is important to highlight that the CLS is used with the deterministic structure presented in (16). As a result, the following parameters are estimated: $\hat{\theta}_1$=1.000000, $\hat{\theta}_2$=6.630913 $\times 10^{-3}$, $\hat{\theta}_3$=−6.157515 $\times 10^{-3}$, and $\hat{\theta}_4$=7.893146. Hence, the combination of these parameter values with structure (16) is symbolized here by $\mathcal{M}_{\mathrm{h},2}$.

Finally, for the same methodology aforementioned, but from a *black-box* perspective, model $\mathcal{M}_{\mathrm{bb}}$ is identified as:

$$y(k) = \hat{\theta}_1 y(k-1) + \hat{\theta}_2 y(k-2) + \hat{\theta}_3 u(k-1), \qquad (17)$$

for which $\hat{\theta}_1$=1.331425, $\hat{\theta}_2$=−3.407265 $\times 10^{-1}$, and $\hat{\theta}_3$ = 8.692694 $\times 10^{-3}$. The predictive performance achieved for these three identified models evaluated for different sinusoidal inputs is shown in Table 1. Such results indicate that $\mathcal{M}_{\mathrm{bb}}$, a purely *black-box* model, is not able to represent the system. Also, both models $\mathcal{M}_{\mathrm{h},1}$ and $\mathcal{M}_{\mathrm{h},2}$ have better predictive power and their results are very similar.

Table 1. Model performance for sinusoidal excitations $u(k)$=Gsen$(2\pi fk)$, quantified by (12).

Model	f [Hz]	G [μm] 20	30	40
$\mathcal{M}_{\mathrm{h},1}$	0.2	2.6%	2.0%	4.7%
	1.0	2.7%	1.3%	4.1%
	5.0	7.7%	5.0%	3.6%
$\mathcal{M}_{\mathrm{h},2}$	0.2	2.7%	2.4%	4.9%
	1.0	2.7%	1.3%	4.1%
	5.0	7.6%	5.0%	3.6%
$\mathcal{M}_{\mathrm{bb}}$	0.2	14.1%	10.6%	8.6%
	1.0	29.0%	27.4%	26.7%
	5.0	31.4%	30.4%	30.2%

In Fig. 3, the performance of models $\mathcal{M}_{\mathrm{h},1}$ and $\mathcal{M}_{\mathrm{h},2}$ are compared for time-varying inputs that become constant. In steady-state, as $\bar{\phi}_1$=$\bar{\phi}_2$=0, both models become $\bar{y}$=$\Sigma_y \bar{y}$, having only one eigenvalue equals to Σ_y. The instability for $\mathcal{M}_{\mathrm{h},1}$ derives from Σ_y=$\hat{\theta}_1$=1.000099>1. On the other hand, $\mathcal{M}_{\mathrm{h},2}$ was estimated to ensure Σ_y=$\hat{\theta}_1$=1, so that the model has a *continuum of steady-state solutions*, which enables it to remain at a constant value. For this model, a steady-state error of about 0.48 μm (3.2% of the range) is found in Fig.3(b), and of about 0.10 μm (0.7%) in Fig.3(d). Hence, in comparison with the strategy of (Martins and Aguirre, 2016), models that consent to the constraints proposed in (Abreu et al., 2020) could have similar prediction performance, with the benefit of representing the behavior for time-varying inputs that become constant.

4.3 Experimental Results

This section identifies two NARX models for a pneumatic valve, whose results are compared with models that have been addressed by Rakotondrabe (2011) and Abreu et al. (2020) and that are briefly revisited here. For this valve, the input is a voltage signal that after V/I and I/P conversions becomes a pressure signal that changes the output, i.e. its stem position. Likewise, as defined by Abreu et al. (2020), the sampling time is T_{s} = 0.01 s and

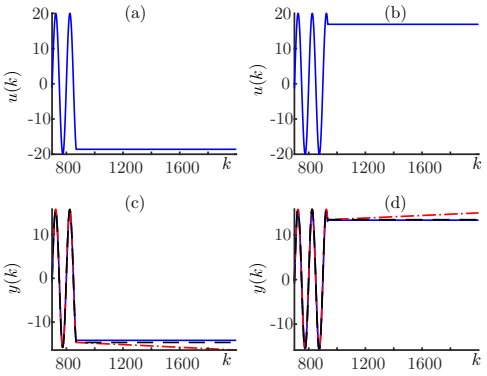

Figure 3. Validation results for $u(k)$=20sen$(4\pi k)$ that becomes constant with final value −18.6 V in (a) and 16.9 V in (b), whose corresponding system output (–) and estimated output of models $\mathcal{M}_{\mathrm{h},1}$ (-·-) and $\mathcal{M}_{\mathrm{h},2}$ (- -) are in (c) and (d), respectively.

the identification input signal is the same used by them, which was generated in a similar way to that proposed in Sec. 3. Specifically, $u(k)$ can be obtained as (10) and (11) with: n=1, f_1=0.1Hz, v=1, o_1=3V, G_1=0.8V, and N=N_1=20000 (200 s long).

For the following two NARX models, the tools used to obtain their structures and parameters are the same as in the previous example, i.e. ERR together AIC and ELS, respectively. Also, it is assumed that ℓ=3, n_y=2 and n_u=1.

1) $\mathcal{M}_{\mathrm{h}}$ refers to the model that includes $\phi_1(k)$ and $\phi_2(k)$, and also adopts the constraints proposed in (Abreu et al., 2020). These constraints are: the exclusion of some regressors showed in (i), (ii) and (iii), and force the parameters to comply with Σ_y=1, see Sec. 2.3. This model is given by:

$$\begin{aligned} y(k)=&\hat{\rho}_1 y(k-1) + \hat{\rho}_2 y(k-2) + \hat{\rho}_3 \phi_1(k-1) \\ &+\rho_4 u(k-1)\phi_1(k-1)\phi_2(k-1) \\ &+\hat{\rho}_5 y(k-2)\phi_1(k-1)\phi_2(k-1), \end{aligned} \qquad (18)$$

with $\hat{\rho}_1 = 9.76\times10^{-1}$, $\hat{\rho}_2 = 2.40\times10^{-2}$, $\hat{\rho}_3 = 1.19\times10^{-1}$, $\hat{\rho}_4 = 3.76$, and $\hat{\rho}_5 = -4.73$. Note that, $\Sigma_y = \hat{\rho}_1 + \hat{\rho}_2 = 1$.

2) $\mathcal{M}_{\mathrm{h,ucs}}$ is identified assuming only the insertion of $\phi_1(k)$ and $\phi_2(k)$ as proposed in (Martins and Aguirre, 2016), so:

$$\begin{aligned} y(k)=&\hat{\theta}_1 y(k-1) + \hat{\theta}_2 y(k-2) + \hat{\theta}_3 u(k-1) \\ &+\hat{\theta}_4 \phi_1(k-1)^2\phi_2(k-1) + \theta_5 y(k-1)u(k-1) \\ &+\theta_6 u(k-1)\phi_1(k-1)\phi_2(k-1) \\ &+\hat{\theta}_7 y(k-2)\phi_1(k-1)\phi_2(k-1), \end{aligned} \qquad (19)$$

where $\hat{\theta}_1 = 9.73\times10^{-1}$, $\hat{\theta}_2 = 2.44\times10^{-2}$, $\hat{\theta}_3 = 1.13\times10^{-3}$, $\hat{\theta}_4$=2.70×10^{2}, $\hat{\theta}_5 = 1.52\times10^{-3}$, $\hat{\theta}_6 = 4.07$, and $\hat{\theta}_7$=−5.18.

Afterward, three models already established in the literature are considered for comparison purposes. The first one is a phenomenological hysteresis model stated below.

3) $\mathcal{M}_{\mathrm{bw}}$ is a Bouc-Wen as in (15). To predict the valve output, its parameters are reestimated with an evolutionary technique described in (Tavares et al., 2019), yielding:

$$\begin{aligned} \dot{h}(t) =& 7.54\times10^{-1}\dot{u}(t) - 4.96|\dot{u}(t)|h(t) - 3.61\dot{u}(t)|h(t)|, \\ y(t) =& 7.21\times10^{-1}u(t) - h(t). \end{aligned} \qquad (20)$$

The last two models below were identified based on the same valve and data set used here, which are taken from (Abreu et al., 2020). However, unlike our strategy, a biased method is used to estimate parameters, and the adopted meta-parameters were ℓ=3, n_y=1 and n_u=2.

4) $\mathcal{M}_{\mathrm{h},2}$ consents with the same constraints used for (18), plus an additional one required by the compensation method to isolate the input (Abreu et al., 2020), yielding:

$$\begin{aligned} y(k)=&y(k-1)-19.76\phi_1(k-2)+19.32\phi_1(k-1)\\ &+9.44\phi_2(k-2)\phi_1(k-2)u(k-2)\\ &-12.61\phi_2(k-2)\phi_1(k-2)y(k-1). \end{aligned} \tag{21}$$

5) $\breve{\mathcal{M}}_{\mathrm{h}}$ is a model that describes the *inverse relationship* between $u(k)$ and $y(k)$. So, the system output $y(k)$ becomes the model input, while the model output is the estimated input $\hat{u}(k)$. Also, the included regressors become: $\breve{\phi}_1(k)=y(k)-y(k-1)$ and $\breve{\phi}_2(k)=\mathrm{sign}[\breve{\phi}_1(k)]$. For the same constraints used for (18), with appropriate conversions for the inverse model, the following model was identified:

$$\begin{aligned} \hat{u}(k)=&\hat{u}(k-1)+86.67\breve{\phi}_1(k-1)-85.02\breve{\phi}_1(k-2)\\ &-0.98\breve{\phi}_1(k-1)y(k-2)+1.72\breve{\phi}_2(k-2)\breve{\phi}_1(k-2)y(k-2)\\ &-1.13\breve{\phi}_2(k-2)\breve{\phi}_1(k-2)\hat{u}(k-1). \end{aligned} \tag{22}$$

The simulation of each model for a sinusoidal input produced the results shown in Fig. 4, in which the left side refers to the results of the directed models and the right side for the inverse model $\breve{\mathcal{M}}_{\mathrm{h}}$. As can be seen, the models provided close results.

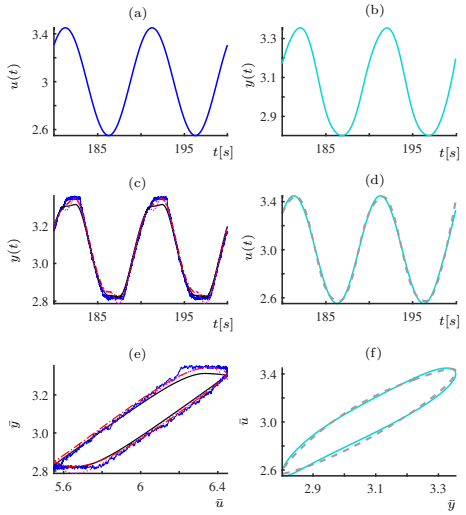

Figure 4. Validation results for the pneumatic valve. Left column refers to the direct models and right column to the inverse model. (a) is the input $u(t) = 0.45\sin(0.2\pi t+\pi/4)+3\,\mathrm{V}$ and the corresponding measured output $y(t)$ (–) and estimated output of models $\mathcal{M}_{\mathrm{h}}$ (- -), $\mathcal{M}_{\mathrm{h,ucs}}$ (-·-), $\mathcal{M}_{\mathrm{bw}}$ (–) and $\mathcal{M}_{\mathrm{h},2}$ (· ·) are in (c); while in (b) is a smoothed version of $y(t)$ in (c), whose corresponding output that is $u(t)$ (–) in (a) and estimated output of inverse model $\breve{\mathcal{M}}_{\mathrm{h}}$ (- -) are in (d). (e) and (f) show the hysteresis loops for the data in (c) and (d), respectively.

A relevant feature is the ability of such models to mimic hysteresis behavior when subjected to a loading-unloading input that, at some point, becomes constant, as considered in Fig. 5. Note that as the input becomes constant during loading and unloading with the same final value (see left side of Fig. 5), the hysteresis behavior leads to different values for the output (Abreu et al., 2020). Also, it is noteworthy that this feature is ensured in the NARX models identified with the constraints revisited in Sec. 2.3 (Abreu et al., 2020). Conversely, without such constraints, the NARX models may diverge over time or converge to a single final value, either during loading or unloading regimes, as seen for $\mathcal{M}_{\mathrm{h,ucs}}$ (19) in Fig. 5(c). The right side of Fig. 5 refers to the results of the inverse model.

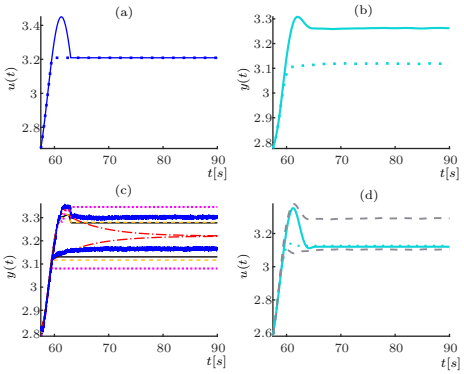

Figure 5. Results of models and valve for a time-varying input that becomes constant. (a) is the input $u(t) = 0.45\sin(0.2\pi t + \pi/4) + 3\,\mathrm{V}$ that becomes constant during loading (· ·) and unloading (–) with final value 3.209V, the corresponding output of valve $y(t)$ (–) and models $\mathcal{M}_{\mathrm{h}}$ (- -), $\mathcal{M}_{\mathrm{h,ucs}}$ (-·-), $\mathcal{M}_{\mathrm{bw}}$ (–) and $\mathcal{M}_{\mathrm{h},2}$ (· ·) are in (c); while in (b) is a smoothed version of $y(t)$ for loading (· ·) and unloading (–) in (c), whose corresponding output that is a smoothed version of $u(t)$ for loading (· ·) and unloading (–) in (a) and output of inverse model $\breve{\mathcal{M}}_{\mathrm{h}}$ (- -) are in (d).

For comparison purposes, the errors mentioned below refer to those in steady-state for the unloading regime. As $\mathcal{M}_{\mathrm{h,ucs}}$ has a single stable fixed point, its output converges to this point resulting in an error of about 0.22 V. The phenomenological model $\mathcal{M}_{\mathrm{bw}}$(20) can hold the output value instantly with an error of about 0.024 V. Models $\mathcal{M}_{\mathrm{h},2}$ (21) and $\breve{\mathcal{M}}_{\mathrm{h}}$ (22) are also able to remain at their last output value when the input becomes constant, since these models are built with the aforementioned constraints. Such models present errors of about 0.043 V and 0.170 V, respectively. These considerable errors are related to the fact that during the transition to steady-state, only the included regressors with delay $k-1$ are immediately canceled. Therefore, as both models have regressors that depend on the instant $k-3$, e.g. $\phi_1(k-2)=u(k-2)-u(k-3)$, and the respective coefficients have high magnitudes, such terms produce sudden changes during transition, giving rise to considerable errors in the steady-state.

To reduce this type of error, some recommendations are provided below. Firstly, note that in comparison with the other NARX models, $\mathcal{M}_{\mathrm{h}}$(18) has lower errors, i.e. 0.020V. It must be stressed that this model is the unique that satisfy the constraints of Sec. 2.3 and is built according to this work. Although in (Abreu et al., 2020) is required $n_u > \tau_d$, note that our models can be identified considering

$n_u = \tau_d = 1$. It is noteworthy that this assumption used in (Abreu et al., 2020) is demanded since the input regressor must be explicit to apply the compensation techniques presented in that paper. As the models obtained in this work do not consent with this constraint, new techniques will be pursued to employ them in a compensation context.

Besides, note that model $\mathcal{M}_{\mathrm{h}}(18)$ has parameters with lower magnitudes when compared with $\mathcal{M}_{\mathrm{h},2}$ and $\breve{\mathcal{M}}_{\mathrm{h}}$. The parameters of the models identified by Abreu et al. (2020) were estimated with a biased method. It suggests that the use of methods that avoid the parameter polarization and the appropriate choice of meta-parameters ($n_u = \tau_d = 1$), as considered in this work, presents a promising way to reduce such errors in steady-state.

5. CONCLUSION

This work has described a concise mathematical formulation for designing excitation signals. In this design, it is possible to select the frequency range where most spectral energy is concentrated and the operation regions where the system will be driven.

A number of practical aspects in the identification of hysteretic systems has been discussed. In particular, the effect of constraints proposed in Abreu et al. (2020) is detailed. It is shown that without such constraints the model behavior under loading and unloading is not correct. Another aspect that has been investigated is that of unbiased parameter estimation in conjunction with an appropriate selection of identification meta-parameters. It has been shown that following such recommendations yields models with lower errors in steady-state.

The discussions have been made in the context of three examples. The obtained models, which have simple structure with no more than 5 terms, are not compatible with the methods proposed in (Abreu et al., 2020) for compensation purposes. For this reason, a new technique was recently developed by (Tavares et al., 2020, 2021, in press) to circumvent this issue where these identified models are used.

REFERENCES

Abreu, P.E.O.G.B., Tavares, L.A., Teixeira, B.O.S., and Aguirre, L.A. (2020). Identification and nonlinearity compensation of hysteresis using NARX models. *Nonlinear Dynamics*, 102(1), 285–301.

Aguirre, L.A. (2019). A Bird's Eye View of Nonlinear System Identification. *arXiv:1907.06803 [eess.SY]*.

Aguirre, L.A., Coelho, M.C.S., and Corrêa, M.V. (2005). On the interpretation and practice of dynamical differences between Hammerstein and Wiener models. *Proc. IEE Part D: Control Theory and Applications*, 152(4), 349–356.

Aguirre, L.A., Corrêa, M., and Cassini, C.C.S. (2002). Nonlinearities in NARX polynomial models: representation and estimation. *Proc. IEE Part D: Control Theory and Applications*, 149(4), 343–348.

Aguirre, L.A. and Mendes, E.M.A.M. (1996). Global Nonlinear Polynomial Models: Structure, Term Clusters and Fixed Points. *International Journal of Bifurcation and Chaos*, 6(2), 279–294.

Akaike, H. (1974). A New Look at the Statistical Model Identification. *IEEE Transactions on Automatic Control*, 19(6), 716–723.

Billings, S.A. (2013). *Nonlinear system identification: NARMAX methods in the time, frequency, and spatio-temporal domains*. John Wiley & Sons.

Billings, S.A. and Chen, S. (1989). Extended model set, global data and threshold model identification of severely nonlinear systems. 50(5), 1897–1923.

Draper, N.R. and Smith, H. (1998). *Applied regression analysis*. John Wiley & Sons, New York, 3 edition.

Householder, A.S. (1958). Unitary triangularization of a nonsymmetric matrix. *Journal of the ACM (JACM)*, 5(4), 339–342.

Ikhouane, F. and Rodellar, J. (2007). *Systems with Hysteresis: Analysis, Identification and Control Using the Bouc-Wen Model*. John Wiley & Sons.

Korenberg, M. et al. (1987). Orthogonal parameter estimation algorithm for non-linear stochastic systems. *Journal of Control*, 48, 193–210.

Leontaritis, I.J. and Billings, S.A. (1985). Input-output parametric models for nonlinear systems part I: Deterministic nonlinear systems. 41(2), 303–328.

Lin, C., Yau, H., and Tian, Y. (2013). Identification and Compensation of Nonlinear Friction Characteristics and Precision Control for a Linear Motor Stage. *IEEE/ASME Transactions on Mechatronics*, 18(4), 1385–1396.

Ljung, L. (1999). *System Identification: Theory for the User*. Prentice Hall, New Jersey, 2 edition.

Martins, S.A.M. and Aguirre, L.A. (2016). Sufficient Conditions for Rate-Independent Hysteresis in Autoregressive Identified Models. *Mechanical Systems and Signal Processing*, 75, 607–617.

Meng, D., Xia, P., Lang, K., Smith, E.C., and Rahn, C.D. (2020). Neural network based hysteresis compensation of piezoelectric stack actuator driven active control of helicopter vibration. *Sensors and Actuators A: Physical*, 302, 111809.

Rakotondrabe, M. (2011). Bouc-Wen Modeling and Inverse Multiplicative Structure to Compensate Hysteresis Nonlinearity in Piezoelectric Actuators. *IEEE Transactions on Automation Science and Engineering*, 8(2), 428–431.

Schoukens, J. and Ljung, L. (2019). Nonlinear system identification: A user-oriented road map. *IEEE Control Systems Magazine*, 39(6), 28–99.

Tavares, L.A., Abreu, P.E.O.G.B., and Aguirre, L.A. (2019). Estimação de Parâmetros de Modelos Bouc-Wen via Algoritmos Evolutivos para Compensação de Histerese. In *Anais do 14º Simpósio Brasileiro de Automação Inteligente*. doi:10.17648/sbai-2019-111154.

Tavares, L.A., Abreu, P.E.O.G.B., and Aguirre, L.A. (2020). Nonlinearity Compensation Based on Identified NARX Polynomials Models. *arXiv:2011.12246 [eess.SY]*.

Tavares, L.A., Abreu, P.E.O.G.B., and Aguirre, L.A. (2021, in press). Nonlinearity Compensation Based on Identified NARX Polynomials Models. *Nonlinear Dynamics*.